Vibrational ratchets

M. Borromeo[1] and F. Marchesoni[2]

[1]*Dipartimento di Fisica, Università di Perugia,*
I-06123 Perugia, Italy and Istituto Nazionale di Fisica Nucleare, Sezione di Perugia, I-06123 Perugia, Italy
[2]*Dipartimento di Fisica, Università di Camerino, I-62032 Camerino, Italy*

Transport in one-dimensional symmetric devices can be activated by the combination of thermal noise and a biharmonic drive. For the study case of an overdamped Brownian particle diffusing on a periodic one-dimensional substrate, we distinguish two apparently different biharmonic regimes: (i) *Harmonic mixing*, where the two drive frequencies are commensurate and of the order of some intrinsic relaxation rate. Earlier predictions based on perturbation expansions seem inadequate to interpret our simulation results; (ii) *Vibrational mixing*, where one harmonic drive component is characterized by high frequency but finite amplitude-to-frequency ratio. Its effect on the device response to either a static or a low-frequency additional input signal is accurately reproduced by rescaling each spatial Fourier component of the substrate potential, separately. Contrary to common wisdom, based on the linear response theory, we show that extremely high-frequency modulations can indeed influence the response of slowly (or dc) operated devices, with potential applications in sensor technology and cellular physiology. Finally, the mixing of two high-frequency beating signal is also investigated both numerically and analytically.

PACS number(s): 05.60.−k, 07.50.Qx, 87.10.+e

I. INTRODUCTION

The spectral density of the response of a system at thermodynamical equilibrium to a sinusoidal time modulation consists of a δ-like spike centered at the forcing frequency. In linear response theory, the system response to two sufficiently weak sinusoidal modulations with different frequency is well reproduced by the linear superposition of the system response to each modulation, separately. In other words, the spectral contents of the system output coincides with that of the input signal. A significant exception is represented by the *harmonic mixing* (HM) of two commensurate input frequencies of comparable magnitude [1]: The system response then can contain harmonics of both drive frequencies and thus, under certain conditions, even a dc component.

In this paper we focus on the regime when at least one drive component is characterized by high frequency but finite amplitude-to-frequency ratio. Such a fast modulation modifies the internal dynamics of the system, so that its response to the other harmonic drive is sensitive to both modulating frequencies, no matter what their ratio. Such a frequency coupling, termed *vibrational mixing*, does not fall within the framework of the linear response theory, as the amplitude of at least one drive component must be appreciably large. Right for this reason, however, the regime investigated here is consistent with the operating conditions of many real devices and is, indeed, of general applicability.

Our study case is represented by a Brownian particle moving on a one dimensional substrate subjected to an external biharmonic force $F(t)$ and a zero mean valued, δ-correlated Gaussian noise $\xi(t)$. Its coordinate $x(t)$ obeys the Langevin equation (LE)

$$\dot{x} = -V'(x) + F(t) + \xi(t), \tag{1}$$

where

$$F(t) = A_1 \cos(\Omega_1 t + \phi_1) + A_2 \cos(\Omega_2 t + \phi_2) \tag{2}$$

with $A_1, A_2 \geq 0$,

$$\langle \xi(t) \rangle = 0, \quad \langle \xi(t)\xi(0) \rangle = 2D\delta(t), \tag{3}$$

and $V(x)$ is the periodic potential of a substrate with period $L = 2\pi$.

In Sec. II we compare the results of extensive numerical simulations with earlier perturbation predictions for the rectification current $\langle \dot{x} \rangle / 2\pi$ induced by HM. We conclude that, in spite of the abundance of numerical results, the analytical description of HM available in the literature is still incomplete and, to some extent, unsatisfactory. We then introduce the vibrational mixing regime. A high-frequency perturbation pumps energy into the system forcing free particle oscillations of amplitude $\psi_0 = A_2 / \Omega_2$ comparable with the system length scale. In Sec. III we demonstrate both numerically and analytically that the particle response to an additional dc drive is extremely sensitive to the high-frequency pump parameter ψ_0. In Sec. IV we extend our approach to investigate the rectification current in a rocked ratchet driven by a biharmonic force with high and low frequency components (vibrational rocked ratchet). Finally, in Sec. V we consider the case of a ratchet driven by two high-frequency beating harmonic forces. We show that in such a limit a vibrational ratchet can be assimilated to a pulsated ratchet, where the modulation frequency of the substrate amplitude corresponds to the drive beating frequency.

II. HARMONIC MIXING

We know from the literature of the 1970's [1] that a charged particle confined onto a nonlinear substrate is capable of mixing two alternating input electric fields of angular frequencies Ω_1 and Ω_2; its response is expected to contain
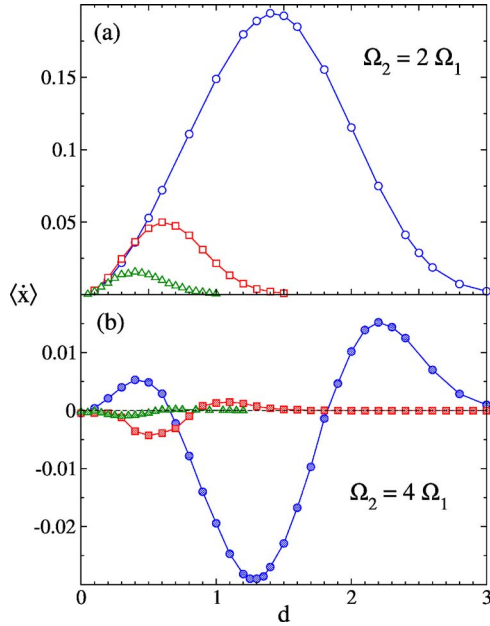
FIG. 1. (Color online) Transport via HM in the cosine potential (5) for $\phi_1 = \phi_2$, $A_1 = A_2$, and (a) $\Omega_2 = 2\Omega_1$, (b) $\Omega_2 = 4\Omega_1$: $\langle \dot{x} \rangle$ versus d. Simulation parameters: $\Omega_1 = 0.01$, $D = 0.2$, and $A_1 = 0.2$ (triangles), $A_1 = 0.4$ (squares), and $A_1 = 1.1$ (circles).

harmonics of Ω_1 and Ω_2. As a result, for commensurate input frequencies, i.e., $m\Omega_1 = n\Omega_2$, the time dependent particle velocity would contain a dc component, too. Such a phenomenon, termed in the later literature *harmonic mixing*, is a rectification effect induced by the asymmetry of the applied force. In view of general perturbation arguments, HM was predicted to be of the $(n+m)$th order in the dynamical parameters of the system [2,3]. Lately, HM was reinterpreted as a manifestation of the ratchet phenomenon [4,5], even if no substrate asymmetry is required to generate a HM signal.

More recently, the HM mechanism has been investigated numerically as a tool to control the transport of interacting particles in artificially engineered quasi-one-dimensional channels [6,7]. An interesting variation of this problem has been proposed in the context of soliton dynamics, where the combination of two ac driving forces was proven to rectify the motion of a kink-bearing chain owing to the inherent nonlinearity of a traveling kink [8].

Let us consider, for simplicity, the overdamped stochastic dynamics (1) driven by the biharmonic force

$$F(t) = A_1 \cos(\Omega_1 t) + A_2 \cos(\Omega_2 t) \tag{4}$$

with

$$V(x) = d(1 - \cos x) \tag{5}$$

and $\Omega_2 = 2\Omega_1$. A truncated continued fraction expansion [2] led to conclude that in the regime of low temperature, $d \gg D$, the nonvanishing dc component $\langle \dot{x} \rangle$ of the particle velocity would scale like
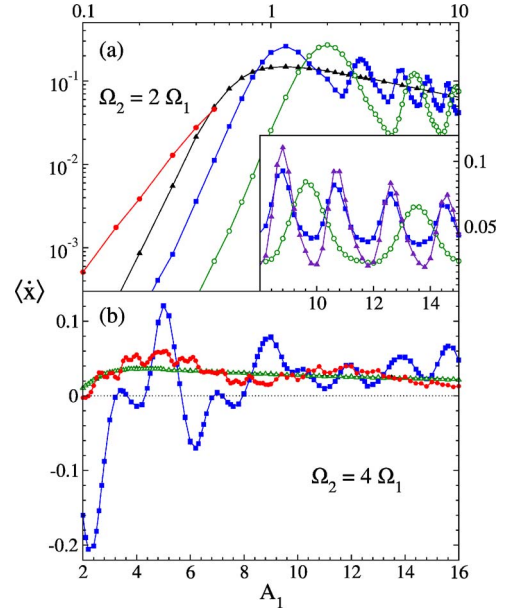
FIG. 2. (Color online) Transport via HM in the cosine potential (5) for $\phi_1 = \phi_2$, $A_1 = A_2$, and (a) $\Omega_2 = 2\Omega_1$, (b) $\Omega_2 = 4\Omega_1$: $\langle \dot{x} \rangle$ versus A_1. Simulation parameters: (a) squares: $\Omega_1 = 0.4$, $D = 0.2$; empty circles: $\Omega_1 = 0.8$, $D = 0.2$; triangles: $\Omega_1 = 0.01$, $D = 0.2$; solid circles: $\Omega_1 = 0.05$, $D = 0.4$. Inset: squares: $\Omega_1 = 0.4$, $D = 0.2$; empty circles: $\Omega_1 = 0.8$, $D = 0.2$; triangles: $\Omega_1 = 0.4$, $D = 0.1$; (b) squares: $\Omega_1 = 0.4$, $D = 0.2$; circles: $\Omega_1 = 0.1$, $D = 0.2$; triangles: $\Omega_1 = 0.01$, $D = 0.2$. In both panels $d = 1$.

$$\frac{\langle \dot{x} \rangle}{D} \propto -\left(\frac{A_1}{2D} \right)^2 \frac{A_2}{2D}. \tag{6}$$

Quite surprisingly, this result suggests that for small drive amplitudes and high substrate barriers, $A_1, A_2 \ll D \ll d$, the HM signal is *negative* and *independent* of d, at variance with the numerical results reported in Fig. 1. Numerical simulation runs for increasing d values reveal a resonant $\langle \dot{x}(d) \rangle$ curve. This is not unexpected as for $d \to 0$ (flattening substrate) the zero-mean force (4), with $\langle F(t) \rangle = 0$, cannot sustain a non-null drift current, whereas for $d \to \infty$ (high substrate barriers) the interwell activation mechanism gets exponentially suppressed and the relevant drift current drops to zero. [The conflicting sign in Eq. (6) is likely to be due to an erroneous definition in Ref. [2].]

The numerical dependence of $\langle \dot{x} \rangle$ on the amplitude of $F(t)$ is also more complicated than expected from the perturbation estimate (6). In Fig. 2 the time average of $\dot{x}(t)$ is plotted versus $A \equiv A_1 = A_2$ at different drive frequencies $\Omega_2 = 2\Omega_1$. For low drive amplitudes the HM signal $\langle \dot{x} \rangle$ grows indeed proportional to A^3, as suggested by the scaling law (6), but only for a sufficiently high noise level D.

Moreover, Fig. 2 illustrates another interesting property of rectification by HM: at relatively high ac frequencies (nonadiabatic regime), the curves $\langle \dot{x}(A) \rangle$ develop regular oscillations for $A > 1$ with period and amplitude roughly proportional to Ω_1. The details of such a nonadiabatic mechanism are explained in Ref. [9]: On setting A at increasingly high values above the depinning threshold of $V(x)$, $\max\{|V'(x)|\}$
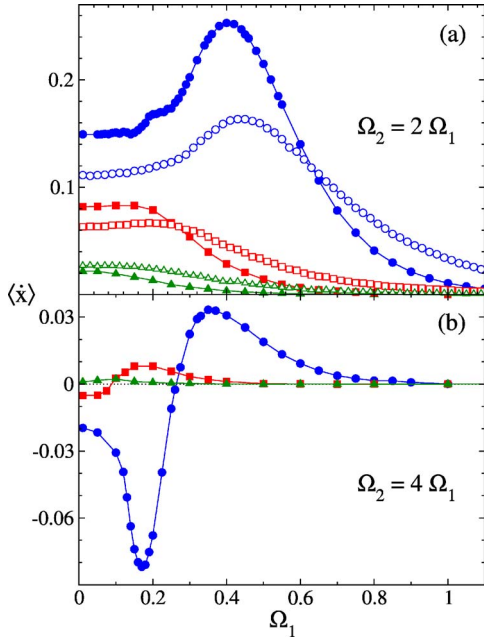
FIG. 3. (Color online) Transport via HM in the cosine potential (5) for $\phi_1 = \phi_2$, $A_1 = A_2$, and (a) $\Omega_2 = 2\Omega_1$, (b) $\Omega_2 = 4\Omega_1$: $\langle \dot{x} \rangle$ versus Ω_1. Simulation parameters: solid symbols: $D = 0.2$; empty symbols: $D = 0.4$; triangles: $A_1 = 0.4$; squares: $A_1 = 0.6$; circles: $A_1 = 1.1$; in both panels $d = 1$.

$= 1$, the number of substrate cells the driven particle crosses during one half-cycle, increases by one unit, first to the right and then to the left, thus causing one full $\langle \dot{x} \rangle$ oscillation at regular A increments, ΔA, proportional to Ω_1. Of course, in the adiabatic limit, $\Omega_1 \to 0$, these oscillations tend to disappear with ΔA. Moreover, shortening the drive period or lowering the noise level for $A > 1$ enhances the above modulation effect [9]. Finally, on further increasing A the cancellation of the right and the left drifts becomes more and more efficient; as a result the envelope of the $\langle \dot{x} \rangle$ oscillations in Fig. 2 decays seemingly inversely proportional to $\sqrt{A}$.

An independent perturbation approach [3] led to the following scaling law for the rectification velocity of a Brownian particle (1) in a cosine potential (5) subject to the harmonic force (4) with $\Omega_2 = 2\Omega_1$

$$\frac{\langle \dot{x} \rangle}{\Omega_1} \propto \left(\frac{d}{D} \right)^2 \left(\frac{A_1}{2\Omega_1} \right)^2 \frac{A_2}{2\Omega_2}. \tag{7}$$

This prediction, that applies under the conditions $d \ll \Omega_1 \ll D$, reproduces at least qualitatively both the $d \to 0$ branches of Fig. 1 and the $\Omega_1 \to \infty$ tails of the curves $\langle \dot{x}(\Omega_1) \rangle$ in Fig. 3. We leave the task of a quantitative assessment of Eq. (7) for future simulation work. Here we limit ourselves to remarking that for large commensurate drive frequencies, i.e., $\Omega_1 = m\Omega_0$ and $\Omega_2 = n\Omega_0$ with $\Omega_0 \to \infty$, the HM signal drops sharply to zero.

We now address two totally different drive regimes that cannot be assimilated to the HM phenomenon introduced above. Having in mind the drive force (4), we consider the limits:
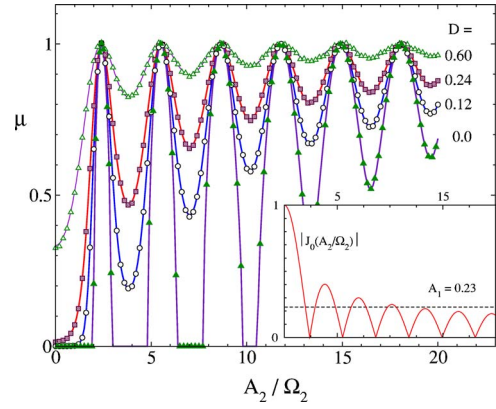
FIG. 4. (Color online) Mobility versus A_2/Ω_2 in the dc case, $\Omega_1 = 0$ and $\phi_1 = 0$, for different D. The simulation data (dots) have been obtained by integrating numerically the LE (1) with $V(x)$ given in Eq. (14) and parameter values: $A_1 = 0.23$ and $\Omega_2 = 0.1$. The solid curves represent the corresponding analytic prediction (11.51) of Ref. [15] for the reduced LE (11). Inset: amplitude $|J_0(A_2/\Omega_2)|$ of $\bar{V}(x)$ (solid curve) compared with the static force A_1.

(i): $\Omega_2 \to \infty$ with Ω_1 and A_2/Ω_2 constant;

(ii): $\Omega_+ \to \infty$ with Ω_-, A_1/Ω_1, and A_2/Ω_2 constant.

Here we have introduced the shorthand notation $\Omega_\pm = \frac{1}{2}(\Omega_1 \pm \Omega_2)$. In (i) the frequency and the amplitude of one harmonic component of $F(t)$ are taken both large, but with constant amplitude-to-frequency ratio; in (ii) the frequency and the amplitude of both harmonic components are taken large with constant amplitude-to-frequency ratios and, additionally, with constant beating frequency $2\Omega_-$. The response of system (1) to an external drive (4) in regime (i) or (ii) can be well reproduced within Bleckman's perturbation scheme, or *vibrational mechanics* [10], outlined in Sec. III. Correspondingly, the ensuing frequency mixing effect discussed below will be termed *vibrational mixing*.

III. THE VIBRATIONAL MECHANICS SCHEME

Let us consider the overdamped Brownian particle (1) with $F(t)$ and $\xi(t)$ defined in Eqs. (2) and (3), respectively. The periodic substrate potential $V(x)$ has period $L = 2\pi$ and general form

$$V(x) = \sum_{n=1}^{\infty} a_n \cos(nx) + \sum_{n=1}^{\infty} b_n \sin(nx), \tag{8}$$

for an appropriate choice of the Fourier coefficients $\{a_n\}$ and $\{b_n\}$.

Let us consider for simplicity the regime (i) of Sec. II, that is we assume that one component of $F(t)$ is slow and the other one is fast, say, $\Omega_1 \ll \Omega_2$; then, following the approach of Refs. [11,12], we can separate

$$x(t) \to x(t) + \psi(t), \tag{9}$$

where, in shorthand notation, from now on $x(t)$ represents a slowly time-modulated stochastic process and $\psi(t)$ is the particle free spatial oscillation

$$\psi(t) = \psi_0 \sin(\Omega_2 t + \phi_2) \qquad (10)$$

with amplitude $\psi_0 = A_2/\Omega_2$. On averaging out $\psi(t)$ over time, the LE for the slow reduced spatial variable $x(t)$ can be written as

$$\dot{x} = -\bar{V}'(x) + A_1 \cos(\Omega_1 t + \phi_1) + \xi(t), \qquad (11)$$

where

$$\bar{V}(x) = \sum_{n=1}^{\infty} a_n J_0(n\psi_0)\cos(nx) + \sum_{n=1}^{\infty} b_n J_0(n\psi_0)\sin(nx). \qquad (12)$$

Here, we made use of the identities $\langle \sin[n\psi(t)]\rangle_t = 0$ and $\langle \cos[n\psi(t)]\rangle_t = J_0(n\psi_0)$, with $J_0(x)$ denoting the Bessel function of zero-order [13]—see also inset of Fig. 4—and $\langle(\cdots)\rangle_t$ representing the time average of the argument $(\cdots)$.

This is an instance of the adiabatic elimination of a fast oscillating observable [14], $\psi(t)$, with *constant* amplitude ψ_0. As a result, the slow observable $x(t)$ diffuses on an effective, or renormalized potential $\bar{V}(x)$ driven by the slow harmonic in Eq. (2), alone. We remark that $\bar{V}(x)$ depends on the ratio $\psi_0 = A_2/\Omega_2$, the amplitude of its nth Fourier component oscillating like $|J_0(n\psi_0)|$. The adiabatic separation (9) for $\Omega_1 \ll \Omega_2$ is tenable as long as the fast oscillation amplitudes are clearly distinguishable with respect to the corresponding Brownian diffusion [14], that is $\langle \psi(t)^2\rangle_t = \frac{1}{2}\psi_0^2 \gg 2Dt_2$ with $t_2 = 2\pi/\Omega_2$ or, equivalently

$$D \ll \frac{A_2}{8\pi}\left(\frac{A_2}{\Omega_2}\right). \qquad (13)$$

In the limit $\Omega_2 \to \infty$ at constant A_2/Ω_2, the approximate LE (11) is expected to be very accurate, regardless of the value of D.

We discuss now a simple application of the vibrational mechanics scheme in the presence of a dc drive, i.e., $\Omega_1 = 0$ and $\phi_1 = 0$. The simplest choice for the substrate potential is

$$V(x) = \cos x, \qquad (14)$$

corresponding to setting $a_1 = 1$ and all the remaining Fourier coefficients a_n, b_n to zero. The reduced problem (11) and (12) describes the Brownian diffusion in a washboard potential with variable tilt A_1 [15].

The observable that best quantifies the response of such a system to the dc input A_1 is the mobility $\mu \equiv \langle \dot{x}\rangle/A_1$. In Fig. 4 we compare the simulation data for the full dynamics (1)–(3) against the analytic predictions for the static limit of the LEs (11) and (12) (i.e., when $\Omega_1 = 0$, $\phi_1 = 0$) at increasing ratios A_2/Ω_2 of the ac component of $F(t)$. The solid curves on display have been obtained by computing the analytic expression (11.51) of Ref. [15] for μ. The agreement between simulation and theory is surprisingly close even for noise intensities above our threshold of confidence (13).

The dependence of the system mobility on the high-frequency input signal is remarkable:

(1) The curves $\mu(A_2/\Omega_2)$ exhibit apparent oscillations with maxima at $\mu = 1$. These peaks clearly correspond to values of $\psi_0 = A_2/\Omega_2$ for which the amplitude of $\bar{V}(x) = J_0(\psi_0)\cos x$ vanishes—see inset of Fig. 4;

(2) For $D = 0$ one can apply Eq. (11.54) of Ref. [15] to predict $\mu = \sqrt{1 - [J_0(A_2/\Omega_2)/A_1]^2}$ for $A_1 \geqslant J_0(A_2/\Omega_2)$, and $\mu = 0$ otherwise. As a consequence, the mobility curve can develop a number of reentrant peaks, one for each side peak of $|J_0(A_2/\Omega_2)|$ higher than A_1 (three in Fig. 4; the peak at zero does not count);

(3) At finite noise intensities, μ is positive definite for any A_2/Ω_2; the mobility peaks are located as in the noiseless case, but grow less and less sharp as D increases;

(4) The reduced LEs (11) and (12) holds good for $A_1 = 0$, too. This implies that, for an appropriate choice of ψ_0, a high-frequency sinusoidal drive $A_2 \cos(\Omega_2 t + \phi_2)$ can neutralize the effective substrate potential $\bar{V}(x)$. Explicit numerical simulations (not shown) substantiate this claim. For instance, the time-averaged probability density $P(x)$ of the stochastic process (1), (3), and (14) flattens out for ψ_0 approaching a zero of the Bessel function $J_0(\psi_0)$.

Properties (1)–(4) fully establish the asymptotic regime $\Omega_2 \to \infty$ at constant A_2/Ω_2 for the dynamics (1).

IV. ROCKED VIBRATIONAL RATCHETS

We consider now a more complicated example that falls under the category of the rocked ratchets [16]. The motion of a Brownian particle on an asymmetric substrate gets rectified when driven by a time-correlated force, either stochastic or periodic [4]. Let the Fourier coefficients of the expansion (8) all be zero but $b_1 = -1$ and $b_2 = -\frac{1}{4}$, i.e.,

$$V(x) = -\sin x - \frac{1}{4}\sin 2x. \qquad (15)$$

The corresponding LE (1) describes a doubly rocked ratchet [7]. For arbitrary input frequencies Ω_1, Ω_2, the rectified current of the system is known to exhibit marked commensuration effects and a complicated dependence on the noise intensity and all forcing parameters [7,17]. We claim here that a well defined adiabatic limit exists for $\Omega_1 \to 0$ and $\Omega_2 \to \infty$ with A_2/Ω_2 constant, as suggested by the separation scheme (9). Following the notation of Refs. [11,12], we term a rocked ratchet operated under such conditions a rocked *vibrational* ratchet (VR).

The results of our simulation work are summarized in Figs. 5 and 6. To explain the persistent oscillations of the curves $\mu(A_2/\Omega_2)$, we write down explicitly the renormalized potential, i.e.

$$\bar{V}(x) = -J_0(\psi_0)\sin x - \frac{1}{4}J_0(2\psi_0)\sin 2x. \qquad (16)$$

As long as our adiabatic elimination procedure applies, the ratchet current $j = \langle \dot{x}\rangle/2\pi$ vanishes in correspondence of the zeros of either Bessel function in Eq. (16), due to the restored symmetry of the effective substrate. On denoting by j_n the nth zero of $J_0(x)$, one predicts the following sequence of mobility zeros:
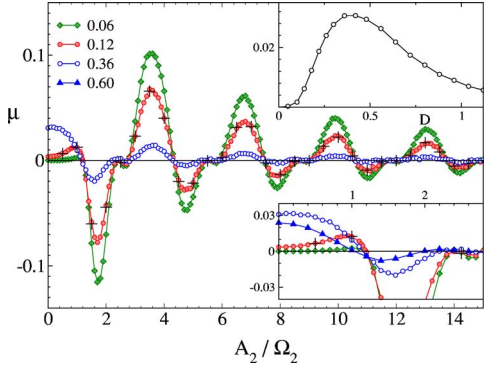
FIG. 5. (Color online) Mobility versus A_2/Ω_2 for the doubly rocked ratchet (1) and (15) with $A_1 = 0.5$, $\Omega_1 = 0.01$, $\phi_1 = \phi_2 = 0$, and different values of the noise intensity D. All simulation data have been obtained for $\Omega_2 = 10$, but the black crosses where we set $D = 0.12$ and $\Omega_2 = 20$. Bottom inset: simulation data for $\mu(A_2/\Omega_2)$ as in the main panel with an additional curve at $D = 0.6$. Top inset: μ versus D for $A_2 = 0$, $A_1 = 0.5$, and $\Omega_1 = 0.01$; circles: simulation data; solid curve: adiabatic formula (11.44) of Ref. [15].

$$\frac{A_2}{\Omega_2} = \frac{1}{2}j_1, j_1, \frac{1}{2}j_2, \frac{1}{2}j_3, j_2, \frac{1}{2}j_4, \frac{1}{2}j_5, j_3, \ldots \quad (17)$$

with $j_1 = 2.405$, $j_2 = 5.520$, $j_3 = 8.654$, $j_4 = 11.79$, $j_5 = 14.93$, etc. [13].

As shown in Fig. 5, the sequence (17) reproduces very closely the zero crossings of our simulation curves for small noise intensities; for $D = 0.06$ we could locate correctly over 20 zeros of the curve $\mu(A_2/\Omega_2)$. In our derivation of the effective potential (16) we cautioned that discrepancies may occur for D above the confidence threshold (13); the deviations observed in the bottom inset of Fig. 5 invalidate our approximation scheme only for $D \gtrsim 1$. The amplitudes of the large $\mu(A_2/\Omega_2)$ oscillations decay like $(A_2/\Omega_2)^{-\frac{1}{2}}$ as expected after noticing that the modulus of $J_0(x)$ vanishes asymptotically like $\sqrt{2/\pi x}$ for $x \to \infty$ [13].
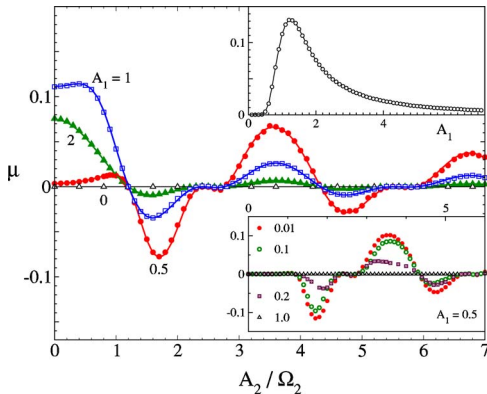
FIG. 6. (Color online) Mobility versus A_2/Ω_2 for the doubly rocked ratchet (1) and (15) with $D = 0.12$, $\Omega_1 = 0.01$, $\Omega_2 = 10$, $\phi_1 = \phi_2 = 0$, and different values of A_1. Top inset: μ versus A_1 for $A_2 = 0$, $D = 0.12$, and $\Omega_1 = 0.01$; circles: simulation; solid curves: adiabatic approximation (11.44) of Ref. [15]. Bottom inset: μ versus A_2/Ω_2 for the for the doubly rocked ratchet (1) and (15) with $A_1 = 0.5$, $D = 0.12$, $\Omega_2 = 10$, $\phi_1 = \phi_2 = 0$, and different Ω_1.

Not all zeros of the sequence (17) mark an inversion of the ratchet current. For instance, for $A_2/\Omega_2 < \frac{1}{2}j_1$ the current in the effective ratchet potential, (11) and (16), is certainly positive in the low Ω_1 frequency regime [16]; for $\frac{1}{2}j_1 < A_2/\Omega_2 < j_1$, the coefficient of $\sin 2x$ changes sign and so does the ratchet polarity (and current); on further increasing A_2/Ω_2 larger than j_1, the sign of both Fourier coefficients (16) get reversed with respect to (15): this is equivalent to turning $V(x)$ upside-down (beside slightly remodulating its profile), so that the polarity of $\bar{V}(x)$ stays negative. Following this line of reasoning one predicts *double* zeros (i.e., no current inversions) at $\psi_0 = j_1, j_2, j_3, j_4, \ldots$.

In the low frequency regime, $\Omega_1 \ll 1$, the reduced ratchet dynamics, (11) and (16), can be treated adiabatically. Its mobility can be computed analytically by time averaging Eq. (11.44) of Ref. [15] over one forcing cycle $t_1 = 2\pi/\Omega_1$. In Fig. 6 the analytic curves for $\mu(A_2/\Omega_2)$ fit very closely our simulation data (dots of the same color) at low noise, no matter what the amplitude A_1 of the slow harmonic in (2). In the bottom inset of Fig. 6 deviations from the low frequency curve become visible for $\Omega_1 \gtrsim 0.1$: this does not imply that the projection scheme leading to the reduced LEs (11) and (12) fails on increasing Ω_1 with $\Omega_1 \ll \Omega_2$, but rather that the adiabatic treatment of the reduced LE becomes untenable. This conclusion is corroborated by the fact that the mobility zeros (and signs) of the curves both in the main panel and in the bottom inset of Fig. 6 are independent of either parameters A_1 and Ω_1 of the low-frequency component.

Figure 6 illustrates another important VR property. In the presence of the high-frequency harmonic, alone, $A_1 = 0$ and $\Omega_2 \gg 1$, the simulated net current is vanishingly small (triangles in the main panel). In the absence of fast oscillations, $A_2 = 0$, instead, the curve $\mu(0)$ versus A_1 is well reproduced by the adiabatic limit $\Omega_1 \ll 1$ [16] (Fig. 6, top inset). On comparison, one notices that, for relatively small A_1, the amplitude of the $\mu(A_2/\Omega_2)$ oscillations can grow notably larger than the corresponding $\mu(0)$. This means that energy pumped into the system at too high a frequency gets dissipated into the heat bath, if the system is operated at equilibrium; vice versa the nonlinear nature of the system induces a cooperative coupling between high-frequency disturbances and optimal drives, thus enhancing the system response beyond the expectations of the linear response theory.

V. PULSATED VIBRATIONAL RATCHETS

We study now the process (1)–(3) in the regime (ii), i.e., for $\Omega_1, \Omega_2 \to \infty$ with $|\Omega_2 - \Omega_1|$, $\psi_1 \equiv A_1/\Omega_1$, and $\psi_2 \equiv A_2/\Omega_2$ constant. In order to simplify the algebraic passages below, we set $\phi_1 = \phi_2$, like in the simulations of Figs. 7–9.

Simple trigonometric manipulations lead to the following expression for the driven free-particle oscillations

$$\psi(t) = (\psi_1 + \psi_2)\sin(\Omega_+ t)\cos(\Omega_- t)$$
$$+ (\psi_1 - \psi_2)\cos(\Omega_+ t)\sin(\Omega_- t), \quad (18)$$
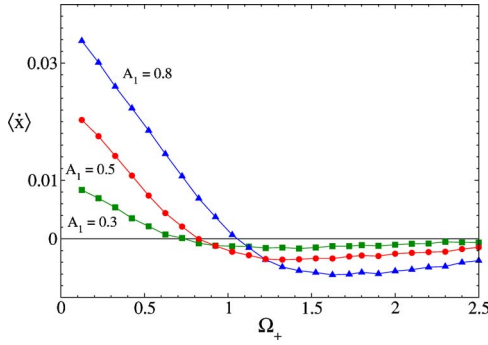
with

FIG. 7. (Color online) Transport in a VR (1) and (15) with D =0.06, Ω_-=0.01, $\phi_1=\phi_2=0$, and different values of $A_1=A_2$: $\langle \dot{x} \rangle$ versus Ω_+.

$$\psi_1 \pm \psi_2 = \frac{\Omega_+(A_1 \pm A_2) - \Omega_-(A_1 \mp A_2)}{\Omega_+^2 - \Omega_-^2}. \qquad (19)$$

The parameter range relevant to the discussion of our simulation results is

$$\frac{A_1 + A_2}{\Omega_+} \gg \left| \frac{A_1 - A_2}{\Omega_-} \right|,$$

so that

$$\psi_1 + \psi_2 \simeq \frac{A_1 + A_2}{\Omega_+} \qquad (20)$$

and

$$\psi_1 - \psi_2 \simeq -\frac{\Omega_-}{\Omega_+^2}(A_1 + A_2), \qquad (21)$$

with $\psi_1 - \psi_2$ negligible with respect to $\psi_1 + \psi_2$.

On applying the vibrational mechanics scheme of Sec. III, the effective LE for the reduced spatial variable $x(t)$ now reads

$$\dot{x} = -\bar{V}'(x,t) + \xi(t), \qquad (22)$$

where
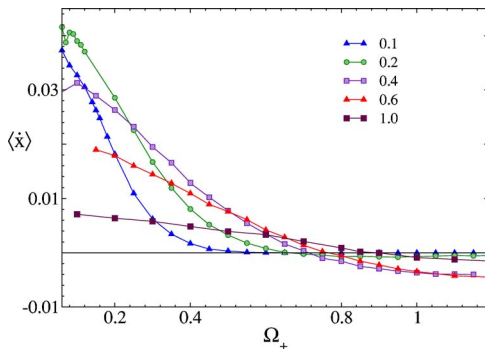
FIG. 8. (Color online) Transport in a VR (1) and (15) with A_1 =A_2=0.5, Ω_-=0.01, $\phi_1=\phi_2=0$, and different values of D: $\langle \dot{x} \rangle$ versus Ω_+.
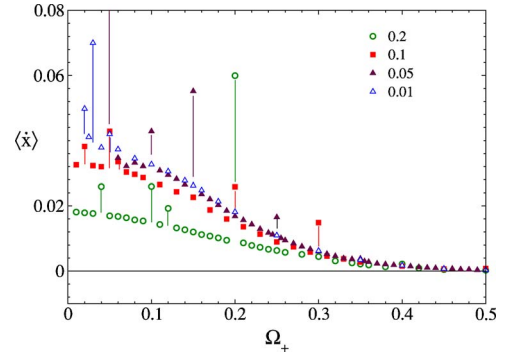
FIG. 9. (Color online) From harmonic to vibrational mixing: $\langle \dot{x} \rangle$ versus Ω_+ in the bi-harmonically rocked ratchet (15) with $A_1=A_2$ =0.5, $\phi_1=\phi_2=0$, and different values of Ω_-=0.01 and D. Spikes appear in correspondence with rational values of Ω_2/Ω_1, i.e., for commensurate harmonic drives.

$$\bar{V}(x,t) = \sum_{n=1}^{\infty} J_0 \left[n \frac{A_1 + A_2}{\Omega_+} \cos(\Omega_- t) \right] [a_n \cos(nx) + b_n \sin(nx)].$$

$$(23)$$

Here we made use of the fact that $|\Omega_-| \ll \Omega_+$, so that the time average $\langle \cos[n\psi(t)] \rangle_t$ could be taken over one fast oscillation cycle $T_+=2\pi/\Omega_+$, while the slow amplitude modulation of period $T_-=2\pi/|\Omega_-|$ was handled as an adiabatic perturbation.

The effect of the biharmonic drive $F(t)$ on the substrate potential is twofold:

(1) The overall amplitude of the periodic function $\bar{V}(x)$ is modulated in time, which is equivalent to periodically modulating the noise intensity D. This condition is reminiscent of the so-called *temperature* ratchets [18] discussed at length in Ref. [4];

(2) Since the argument of the Bessel functions in Eq. (23) depends on the index n, the Fourier coefficients of $\bar{V}(x)$ are distinctly modulated in time; as a consequence, their relative weights change in time and so does the profile of $\bar{V}(x)$.

Separating (sure, rather arbitrarily) the two time dependencies (1) and (2) of $\bar{V}(x)$ helps us explain the simulation results of Figs. 7–9 obtained for the asymmetric potential (15).

Figures 7 and 8 illustrate the most interesting feature of this class of VR, namely the inversion from positive to negative current that takes place for $\Omega_+ \gg |\Omega_-|$. We recall that the positive orientation of $\langle \dot{x} \rangle$ corresponds to the normal polarity of a ratchet (15) slowly rocked by a harmonic drive, whereas the negative orientation is to be expected when the same device is being operated in the pulsated mode (like for an adiabatic temperature ratchet [18]). This is why we term regime (ii) of the process (1)–(3) *pulsated* VR.

Note that the pulsated VR of Figs. 7 and 8 are operated for values of Ω_- and Ω_+ such that the HM mechanism plays no significant role, being the HM spikes confined to values of Ω_+ much closer to $|\Omega_-|$ (as shown in Fig. 9).

The current inversions in the adiabatic regime $\Omega_+ \gg |\Omega_-|$ can be explained by looking at the time-dependent effective potential

$$\bar{V}(x,t) = -J_0\left[\frac{2A}{\Omega_+}\cos(\Omega_- t)\right]\sin(x)$$
$$- \frac{1}{4}J_0\left[\frac{4A}{\Omega_+}\cos(\Omega_- t)\right]\sin(2x), \qquad (24)$$

associated with the substrate potential $V(x)$ of Eq. (15). Here we set $\phi_1 = \phi_2$ and $A_1 = A_2 \equiv A$ to make contact with the simulation conditions of Figs. 7 and 8. For $|4A/\Omega_+| < j_1$, i.e., for $\Omega_+ > \Omega_+^*$ with $\Omega_+^* = 4A/j_1$, both Fourier coefficients in Eq. (24) retain their (negative) sign at any time t; $\bar{V}(x,t)$ does not change polarity and the overall effect of the adiabatic modulation with period T_- amounts to pulsating the amplitude of the effective potential (or, equivalently, the noise level [18]) with the same period. As a consequence, $\langle \dot{x} \rangle$ is predicted to change sign from positive for $\Omega_+ < \Omega_+^*$ to negative for $\Omega_+ > \Omega_+^*$. No more current reversals are expected for higher Ω_+; as usual in the ratchet phenomenology, $\langle \dot{x} \rangle$ tends to zero for $\Omega_+ \to \infty$.

In the actual simulation, see, e.g., Figs. 7 and 8, these current inversions seem to take place for Ω_+ slightly smaller than Ω_+^*. This is due to the fact that at $\Omega_+ = \Omega_+^*$ the second coefficient of Eq. (24) is negative over the entire averaging cycle T_-, but for $t = mT_-$ with $m = 0, 1, 2, \ldots$, where it vanishes. This means that the average $\langle \dot{x} \rangle$ is still negative at $\Omega_+ = \Omega_+^*$ and vanishes only for lower (but not too lower) Ω_+ values, in strict sense, Ω_+^* is only an upper bound to the crossover frequency. This argument applies as long as condition (13) holds; that is not the case of $A_1 = 0.3$ in Fig. 7 and $D = 1.0$ in Fig. 8.

Finally, we note that the dependence of $\langle \dot{x} \rangle$ on the noise intensity D exhibits the resonant behavior peculiar to most ratchet currents [4]. This happens both for positive and negative rectification currents (see Fig. 8).

VI. CONCLUDING REMARKS

The robustness of the effects simulated here hints at the possibility of implementing this concept in the design and operation of efficient electromagnetic (e.m.) wave sensors. As a matter of fact, the present investigation has been inspired by a typical signal detection problem [19], namely how to reveal a high frequency signal by means of a sensor with optimal sensitivity in a relatively low frequency band. All cases discussed in Secs. III–V suggest a simple recipe: Although the unknown high-frequency signal alone cannot be detected, adding a tunable control signal with parameters within the device sensitivity range causes a nonlinear transfer of energy (information) from high to low frequencies, thus enhancing and/or modulating the sensor response to the control signal. By analyzing the dependence of the device output on the tunable input signal, we can reveal the existence of unknown (and otherwise undetectable) high-frequency signals. Note that in the simulations of Figs. 5 and 6 the input frequencies Ω_1 and Ω_2 differ by *four orders* of magnitude or more, whereas the response function μ can be sensitive to forced output oscillation amplitudes ψ_0 as small as the device substrate unit length L. In the simulations of Figs. 7 and 8 instead, the ratchet currents are controlled by beating frequencies $|\Omega_2 - \Omega_1|$ two (or more) orders of magnitude smaller than the carrier frequency $\frac{1}{2}(\Omega_1 + \Omega_2)$.

As a further application we suggest that the mechanism of frequency coupling studied here can impact our assessment of the health hazards associated with electropollution [20]. While high-frequency (nonionizing) e.m. radiation is likely to be harmless at the small length scales of sensitive biomolecules, like the DNA helix [21], still it can affect physiological processes at the cell level. Not only high-frequency e.m. waves heat up the biological tissues, but in view of the present report, such radiation can interfere with the much lower-frequency electrochemical control signals that regulate the ion transport across cell membranes or the information transfer and processing through neuron networks and sensory nerves. In conclusion, our results corroborate the recent shift of the biomedical research focus from structural (and irreversible) to functional (and possibly reversible) biological damages [22] caused by electropollution.

Finally, we mention another potential extension of the vibrational mechanics scheme of Sec. III. In a forthcoming paper we study the inertial effects of the LE

$$\ddot{x} = -\gamma\dot{x} - V'(x) + F(t) + \xi(t) \qquad (25)$$

with $F(t)$ and $\xi(t)$ defined in Sec. I and $D \equiv \gamma kT$. Here we limit ourselves to anticipating that the vibrational mechanics scheme of Sec. II still applies upon replacing $\psi_0 = A_2/\Omega_2$ with

$$\psi_0 \to \psi_\gamma = \frac{\psi_0}{\sqrt{\gamma^2 + \Omega_2^2}}. \qquad (26)$$

As a consequence, $\langle \dot{x} \rangle$ depends on both ψ_0 and Ω_2, which suggests the design of highly sensitive devices capable of separating the components of a multispecies mixture according to the different particle masses.

[1] K. Seeger and W. Maurer, Solid State Commun. **27**, 603 (1978).

[2] W. Wonneberger and H. J. Breymayer, Z. Phys. B: Condens. Matter **43**, 329 (1981).

[3] F. Marchesoni, Phys. Lett. A **119**, 221 (1986); M. Borromeo and F. Marchesoni, Europhys. Lett. **68**, 783 (2004).

[4] P. Reimann, Phys. Rep. **361**, 57 (2002); P. Hänggi, F. Marchesoni, and F. Nori, Ann. Phys. **14**, 51 (2005); L. Gammaitoni, P. Hänggi, P. Jung, and F. Marchesoni, Rev. Mod. Phys. **70**, 223 (1998).

[5] S. Flach, O. Yevtushenko, and Y. Zolotaryuk, Phys. Rev. Lett. **84**, 2358 (2000); S. Denisov and S. Flach, Phys. Rev. E **64**, 056236 (2001).

[6] S. Savel'ev, F. Marchesoni, and F. Nori, Phys. Rev. Lett. **91**,

010601 (2003); **92**, 160602 (2004).

[7] S. Savel'ev, F. Marchesoni, P. Hänggi, and F. Nori, Europhys. Lett. **67**, 179 (2004); Phys. Rev. E **70**, 066109 (2004); Europhys. Lett. **40**, 403 (2004).

[8] L. Morales-Molina, N. R. Quintero, F. G. Mertens, and A. Sànchez, Phys. Rev. Lett. **91**, 234102 (2003); A. L. Sukstanskii and K. I. Primak, Phys. Rev. Lett. **75**, 3029 (1995); Yu. S. Kivshar and A. Sànchez, Phys. Rev. Lett. **77**, 582 (1996); M. Salerno and Y. Zolotaryuk, Phys. Rev. E **65**, 056603 (2002); F. Marchesoni, Phys. Rev. Lett. **77**, 2364 (1996); A. V. Ustinov, C. Cogui, A. Kemp, Y. Zolotaryuk, and M. Salerno, Phys. Rev. Lett. **93**, 087001 (2004).

[9] M. Borromeo, G. Costantini, and F. Marchesoni, Phys. Rev. E **65**, 041110 (2002).

[10] I. I. Bleckman, *Vibrational Mechanics* (World Scientific, Singapore, 2000).

[11] P. S. Landa and P. V. E. McClintock, J. Phys. A **33**, L433 (2000).

[12] A. A. Zaikin, L. Lopez, J. P. Baltanás, J. Kurths, and M. A. F. Sanjuan, Phys. Rev. E **66**, 011106 (2002); J. P. Baltanás, L. Lopez, I. I. Blechman, P. S. Landa, A. Zaiken, J. Kurths, and M. A. F. Sanjuan, Phys. Rev. E **67**, 066119 (2003); E. Ullner *et al.*, Phys. Lett. A **312**, 348 (2003); J. Casado-Pascual and J. P. Baltanás, Phys. Rev. E **69**, 046108 (2004); M. Borromeo and F. Marchesoni, Europhys. Lett. **72**, 362 (2005).

[13] *Handbook of Mathematical Functions*, edited by M. Abramowitz and I. Stegun (London, Dover, 1972).

[14] F. Marchesoni and P. Grigolini, Physica A **121**, 269 (1983); Z. Phys. B: Condens. Matter **55**, 257 (1984).

[15] H. Risken, *The Fokker-Planck Equation* (Springer, Berlin, 1984), Chap. 11.

[16] R. Bartussek, P. Hänggi, and J. P. Kissner, Europhys. Lett. **28**, 459 (1994).

[17] M. Borromeo and F. Marchesoni, Chaos **15**, 026110 (2005).

[18] P. Reimann, R. Bartussek, R. Häussler, and P. Hänggi, Phys. Lett. A **215**, 26 (1996); see also A. A. Dubkov and B. Spagnolo, Phys. Rev. E **72**, 041104 (2005).

[19] See, e.g., S. W. Smith, *Digital Signal Processing* (San Diego, California Tech. Publ., 1997); A. Yariv, *Quantum Electronics* (New York, Wiley, 1988).

[20] See, e.g., A. Ahlbom *et al.*, Health Phys. **74**, 494 (1998).

[21] R. S. Malyapa *et al.*, Radiat. Res. **149**, 637 (1998).

[22] *Biological coherence and response to external stimuli*, edited by H. Fröhlich (Berlin, Springer, 1988).